AGU PUBLICATIONS

Global Biogeochemical Cycles

RESEARCH ARTICLE
10.1002/2015GB005276

Key Points:
- Satellite-retrieved phytoplankton carbon shows similar annual cycles across subarctic ocean basins
- Phytoplankton physiological changes mitigate the annual biomass signal in the chlorophyll record
- Biomass accumulation rates in both basins are closely tied to nutrient drawdown

Supporting Information:
- Texts S1–S5 and Figures S1–S5

Correspondence to:
T. K. Westberry,
toby.westberry@science.oregonstate.edu

Citation:
Westberry, T. K., M. J. Behrenfeld, P. Schultz, J. P. Dunne, M. R. Hiscock, S. Maritorena, J. L. Sarmiento, and D. A. Siegel (2016), Annual cycles of phytoplankton biomass in the subarctic Atlantic and Pacific Ocean, *Global Biogeochem. Cycles*, *30*, 175–190, doi:10.1002/2015GB005276.

Received 3 SEP 2015
Accepted 5 JAN 2016
Accepted article online 7 JAN 2016
Published online 5 FEB 2016
Corrected 24 FEB 2016

This article was corrected on 24 FEB 2016. See the end of the full text for details.

©2016. American Geophysical Union. All Rights Reserved.

Annual cycles of phytoplankton biomass in the subarctic Atlantic and Pacific Ocean

Toby K. Westberry[1], Patrick Schultz[2], Michael J. Behrenfeld[1], John P. Dunne[3], Michael R. Hiscock[2], Stephane Maritorena[4], Jorge L. Sarmiento[2], and David A. Siegel[4]

[1]Department of Botany and Plant Pathology, Oregon State University, Corvallis, Oregon, USA, [2]Atmospheric and Oceanic Sciences Program, Princeton University, Princeton, New Jersey, USA, [3]Geophysical Fluid Dynamics Laboratory, NOAA, Princeton, New Jersey, USA, [4]Earth Research Institute, University of California, Santa Barbara, California, USA

Abstract High-latitude phytoplankton blooms support productive fisheries and play an important role in oceanic uptake of atmospheric carbon dioxide. In the subarctic North Atlantic Ocean, blooms are a recurrent feature each year, while in the eastern subarctic Pacific only small changes in chlorophyll (Chl) are seen over the annual cycle. Here we show that when evaluated using phytoplankton carbon biomass (C_{phyto}) rather than Chl, an annual bloom in the North Pacific is evident and can even rival blooms observed in the North Atlantic. The annual increase in subarctic Pacific phytoplankton biomass is not readily observed in the Chl record because it is paralleled by light- and nutrient-driven decreases in cellular pigment levels (C_{phyto}:Chl). Specifically, photoacclimation and iron stress effects on C_{phyto}:Chl oppose the biomass increase, leading to only modest changes in bulk Chl. The magnitude of the photoacclimation effect is quantified using descriptors of the near-surface light environment and a photophysiological model. Iron stress effects are diagnosed from satellite chlorophyll fluorescence data. Lastly, we show that biomass accumulation in the Pacific is slower than that in the Atlantic but is closely tied to similar levels of seasonal nutrient uptake in both basins. Annual cycles of satellite-derived Chl and C_{phyto} are reproduced by in situ autonomous profiling floats. These results contradict the long-standing paradigm that environmental conditions prevent phytoplankton accumulation in the subarctic Northeast Pacific and suggest a greater seasonal decoupling between phytoplankton growth and losses than traditionally implied. Further, our results highlight the role of physiological processes in shaping bulk properties, such as Chl, and their interpretation in studies of ocean ecosystem dynamics and climate change.

1. Introduction

The high-latitude seasonal seas control large fluxes of heat, momentum, and radiatively important gases to and from the atmosphere [*Broecker*, 1991; *Broecker and Denton*, 1990; *Takahashi et al.*, 1995, 2009; *Warren*, 1983]. They also support productive fisheries and play a critical role in elemental cycling. A defining characteristic of nearly all these regions is that they exhibit strong ecological and biogeochemical seasonality that is intimately related to strong annual cycles in meteorological and water column properties (e.g., incident light, sea surface temperature, and wind forcing). These physical forcings drive a diversity of ecosystem responses, but a common feature is annually recurrent phytoplankton blooms [e.g., *Colebrook*, 1982; *Henson et al.*, 2009; *Martinez et al.*, 2011]. Many marine species, such as copepods, other crustaceans, and larval fish, have evolved life cycles finely tuned to their regional cycle of phytoplankton bloom and decline [*Koeller et al.*, 2009; *Platt et al.*, 2003]. The regularity of the spring bloom is often qualitatively compared—albeit incorrect mechanistically—to the spring flush of terrestrial vegetation in temperate boreal forests (see discussion in *Behrenfeld and Boss* [2014]).

In the Northern Hemisphere, the subarctic Atlantic hosts the classic example of seasonal plankton blooms. The extent and recurrence of this bloom have been thoroughly described using merged satellite data spanning a 30+ year record [*Martinez et al.*, 2011] and coupled ocean ecosystem modeling over an even longer time period [*Henson et al.*, 2009]. The high-nitrate, low-chlorophyll (HNLC) region of the subarctic Northeast Pacific Ocean provides a stark contrast to the subarctic Atlantic. In this Pacific environment, macronutrient concentrations never reach the limiting levels found in the summertime North Atlantic or the subtropical oceans. Furthermore, chlorophyll concentrations (Chl) in the subarctic Northeast Pacific are relatively invariant throughout the year, leading to the commonly held view that this region lacks a seasonal phytoplankton bloom altogether. The contrasting chlorophyll cycles in the subarctic Pacific and Atlantic basins were well described in the classic works by *Parsons and Lalli* [1988] and *Evans and Parslow* [1985].

Many early field studies on phytoplankton were carried out in the North Atlantic Ocean (NAtl), owing in part to its proximity to western Europe and the eastern United States. The observations of *Gran and Braarud* [1935] and *Sverdrup* [1953] formed the basis of the traditional "bottom-up" interpretation of seasonal phytoplankton blooms. In this scenario, macronutrients are entrained into surface waters by deep winter mixing and then thermal stratification during spring improves growth conditions for the light-limited (not nutrient limited) phytoplankton, resulting in a "spring bloom" [*Sverdrup*, 1953]. The regularly observed rise in surface pigment concentrations (volumetric) from winter to spring and their climax in late spring are often viewed as evidence supporting this bottom-up interpretation. However, recent work has challenged this simplistic picture and emphasized instead that the factors decoupling phytoplankton division and loss rates are the fundamental drivers of the annual cycle of bloom and demise [*Behrenfeld and Boss*, 2014]. Thus, the mechanisms underpinning bloom regulation are still actively being investigated [*Behrenfeld*, 2010; *Brody and Lozier*, 2014; *Chiswell et al.*, 2015; *Taylor and Ferrari*, 2011].

The subarctic North Pacific Ocean (NPac) has been the site of several large oceanographic programs during the twentieth century. The weathership era (~1946–1980), which established Ocean Station Papa (OSP) in the central Gulf of Alaska at 145°W, 50°N, was a period of time when the primary goal of ocean-going research vessels was collecting meteorological data for weather forecasting [*Freeland*, 2007]. The weathership program included a limited number of oceanographic observations (e.g., Chl) but with very good temporal resolution throughout the year. In contrast, cruises to OSP during the modern era occur only two or three times per year but measure a broad suite of biogeochemical quantities. In addition to these sustained programs, the region around OSP has also hosted a number of targeted process studies designed to address issues such as iron limitation (Vertical Transport and Exchange Study (VERTEX)) [*Martin and Fitzwater*, 1988], grazing control of phytoplankton (SUbarctic Pacific Ecosystem Research, SUPER) [*Miller et al.*, 1991], and carbon cycling (Canadian-Joint Global Ocean Flux Study (C-JGOFS)) [*Boyd et al.*, 1999]. Well-defined annual cycles in many ecosystem properties have been documented [*Whitney and Freeland*, 1999; *Wong et al.*, 1999], but the limited range of variability of one property in particular, Chl, has disproportionately shaped our understanding of phytoplankton phenology at OSP.

The general stability of chlorophyll concentrations in the subarctic Northeast Pacific is perhaps best appreciated by recognizing that the average annual winter-to-summer increase requires only a single doubling in Chl over a ~6 month period. In light of this modest annual cycle, the emergent consensus has been that the region lacks an annual bloom because small species outcompete larger bloom-forming taxa for iron but are themselves prevented from blooming because of rapid losses to microzooplankton grazing [*Harrison*, 2002]. This tight coupling between smaller phytoplankton and microzooplankton is perpetuated through winter by sustained algal production in a comparatively shallow surface mixing layer. Thus, unique physical, chemical, and ecosystem attributes of the eastern subarctic Pacific are thought to create the tight controls on phytoplankton biomass, thereby preventing blooms and impacting nitrate drawdown and carbon export. However, recent work that aimed at better understanding controls on bloom formation [*Behrenfeld and Boss*, 2014; *Behrenfeld et al.*, 2013] suggests that a reevaluation of annual cycles in phytoplankton in the North Pacific may be warranted.

Here we use satellite retrievals of phytoplankton pigment concentration (Chl) and carbon biomass (C_{phyto}) to evaluate plankton stocks and physiological rates over the annual cycle in the subarctic Pacific and Atlantic. We show that seasonal cycles in C_{phyto} for the two basins are far more similar than conveyed by the Chl record. We propose that the pronounced seasonal cycle in biomass is masked in the Chl record because of simultaneous physiological responses to light and nutrient conditions (in particular, the effects of iron stress on cellular pigmentation). Differences in iron stress for the two basins are further diagnosed using satellite chlorophyll fluorescence data. Finally, calculation of net population growth rates supports a consistent picture of seasonally significant phytoplankton biomass accumulation in the Northeast Pacific, as does the annual pattern of nutrient drawdown. Our interpretation of satellite products is corroborated by in situ data from optical profiling floats and historical climatological data sets.

2. Methods

2.1. Satellite Products

Satellite ocean color products were taken from the Moderate Resolution Imaging Spectroradiometer sensor on Aqua (MODISA) and downloaded directly from the ocean color web portal (http://oceancolor.gsfc.nasa.

gov/). Archive level products used here include chlorophyll concentration (Chl, mg m^{-3}), daily incident broadband irradiance PAR, einstein m^{-2} d^{-1}), instantaneous irradiance at the time of the satellite measurement (iPAR, μE m^{-2} s^{-1}), diffuse attenuation at 490 nm (Kd490, m^{-1}), and fluorescence line height (FLH, mW cm^{-2} sr^{-1} nm^{-1}). Additionally, MODIS multispectral remote sensing reflectance (Rrs(λ), sr^{-1}) was used to estimate Chl and the particulate backscattering coefficient at 443 nm (bbp443, m^{-1}) following the model of *Maritorena et al.* [2002]. This provides an independent estimate of Chl that is free from ocean color biases due to absorption by colored dissolved and detrital matter [e.g., *Siegel et al.*, 2005] and is the preferred Chl product used in our analyses. bbp443 was subsequently used to estimate phytoplankton carbon biomass (C_{phyto}, mg m^{-3}) as in *Behrenfeld et al.* [2005] and *Westberry et al.* [2008]. The relationship between bbp443 and C_{phyto} assumes a linear conversion between the two properties after removal of a nonvarying background value and has been independently validated using novel-sorting flow cytometry methods [*Graff et al.*, 2012, 2015]. Net primary production (NPP) rates (mg C m^{-2} d^{-1}) were calculated with the Vertically Generalized Production Model (VGPM) [*Behrenfeld and Falkowski*, 1997] and the Carbon-based Production Model (CbPM) [*Westberry et al.*, 2008]. Diffuse attenuation for broadband irradiance (K_{PAR}, m^{-1}) was estimated from Kd490 following *Morel et al.* [2007].

All satellite products were downloaded as, or calculated with 8 day, level 3 data, which have a ~9 km pixel size at the equator. Ten full years of data (reprocessing version 2013.1) from the period January 2003 to December 2012 were used for this study. Equally sized 5° × 10° study regions (~550 km × 750 km) were chosen for detailed satellite analyses, 45–50°N, 25–35°W in the North Atlantic and 45–50°N, 140–150°W in the North Pacific, respectively. Both regions are close to historically occupied oceanographic stations, the JGOFS NABE site (47°N, 20°W) in the North Atlantic and Ocean Station Papa (50°N, 145°W) in the North Pacific. In the NAtl, this box corresponds to the central bin (NA-5) in the analysis of *Behrenfeld* [2010].

2.2. Climatological and Modeled Fields

Climatological fields of the macronutrient nitrate (NO_3, μ*M*) were taken from the World Ocean Atlas (WOA) 2009 [*Garcia et al.*, 2010]. These data are gridded to 1° × 1° globally and are provided as monthly climatological values. While WOA data coverage can be sparse for the subarctic North Pacific and North Atlantic, we find that the climatological patterns in this data set are reproduced well by continuously measured NO_3 from profiling floats (see next section).

Another globally gridded product used here is surface mixed layer depth (MLD, m). A singular source for calculating MLD spanning the MODIS time period in a consistent, global, temporally resolved way at the spatial scale required does not exist. Therefore, a merged MLD product was created from numerical output of three distinct sources: the Simple Ocean Data Assimilation model [*Carton et al.*, 2000a, 2000b] from 2002 to 2004, the Fleet Numerical Meteorology and Oceanography Center model [*Clancy and Sadler*, 1992] from 2004 to 2005, and the Hybrid Coordinate Ocean Model [*Bleck*, 2002] from 2005 to 2012. In all cases, MLD was calculated as the depth at which the potential density (σ_θ) exceeded a surface reference value (generally 10 m) by 0.125 kg m^{-3}. An in-depth comparison of each data source and description of their merging can be found at http://www.science.oregonstate.edu/ocean.productivity/mld.html.

2.3. Float Data

Time series data of upper water column Chl fluorescence, bbp443, and NO_3 were collected from APEX-style profiling floats in the North Pacific basin (our comparable floats in the North Atlantic failed shortly after deployment). Chlorophyll fluorescence was converted to Chl concentration (mg m^{-3}) using a fixed, predeployment calibration. Profiles were only collected at nighttime (~2:00 A.M. local time) to minimize light-dependent quenching variability. bbp443 was calculated from measurements of the volume scattering function at 140° following *Boss and Pegau* [2001] and *Dall'Olmo et al.* [2009]. Some shared aspects of sensor calibration (e.g., dark current offsets) followed previous deployments of similar floats and are described in *Boss et al.* [2008]. Long-term stability of deep water Chl and bbp443 values was excellent with minimal variability (supporting information Figure S1). The float was deployed in a "park and profile" mode, sampling at a variable frequency while ascending from its nominal parking depth (~1000 m), telemetering data while at the surface, then returning to a Lagrangian drift at the parking depth. The sampling/profiling frequency was every 4 days from February 2010 to December 2012, resulting in 358 profiles over a ~3 year time period. Data from additional floats located near Station Papa were also used for our analyses that

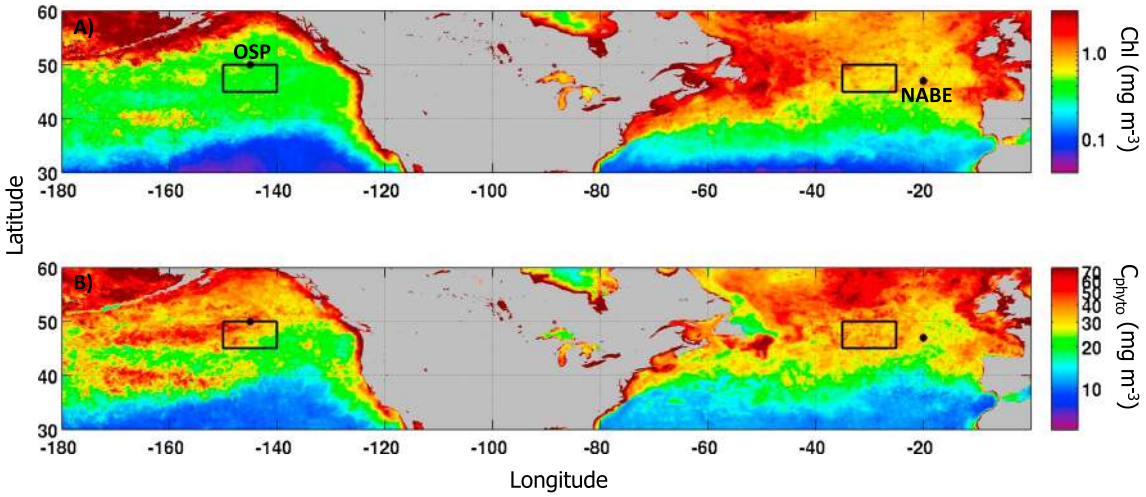

Figure 1. Climatological spring/summer patterns in phytoplankton pigment and carbon biomass. (a) Chlorophyll concentration (Chl, mg m^{-3}). (b) Phytoplankton biomass (C_{phyto}, mg m^{-3}). Values at each pixel are the maximum climatological mean (2003–2012) between April and August from MODIS on Aqua. Black boxes in Pacific and Atlantic are 5° × 10° and centered on 47.5°N, 145°W and 47.5°N, 30°W in the Pacific and Atlantic, respectively. Also shown as solid circles are nearby Station P (50°N, 145°W) and NABE (47°N, 20°W) sites.

provided similar Chl fluorescence and bbp443 estimates and additional measurements of NO_3 concentration. These data are freely available via the Monterey Bay Aquarium Research Institute (MBARI) Chemical Sensor Lab—www.mbari.org/chemsensor/FloatList.html [e.g., *Johnson et al.*, 2010].

3. Results

Climatological summertime (June–August) distributions of Chl and C_{phyto} for the Northern Hemisphere subtropics and subpolar regions are shown in Figures 1a and 1b. Overall, these data indicate a much larger range in Chl values (~100×, 0.03–3.0 mgChl m^{-3}) than carbon biomass values (~10×, 7–70 mgC m^{-3}). At lower latitudes (<40°N), both Chl and C_{phyto} are broadly consistent between the Pacific and Atlantic Oceans. However, at higher latitudes the two basins differ significantly. Typical summertime Chl values in the NAtl (>45°N) are ~1 mgChl m^{-3}, while in the NPac they are ~0.3 mgChl m^{-3}. Spatial heterogeneity in Chl (σ_{chl} is calculated as standard deviation over bounding boxes outlined in Figure 1) is also much larger in the NAtl (σ_{Chl} = 0.3 mgChl m^{-3}) than in the NPac (σ_{Chl} = 0.07 mgChl m^{-3}). Summertime concentrations of phytoplankton biomass (C_{phyto}), on the other hand, are similar between the two subarctic basins, with values ranging from ~30 to 70 mgC m^{-3} for the NAtl and from ~30 to 50 mgC m^{-3} for the NPac (Figure 1b). In other words, the satellite C_{phyto} data suggest that the subarctic Northeast Pacific hosts summertime phytoplankton blooms comparable in magnitude to those observed in regions of the subarctic Atlantic.

The contrasting patterns of Chl and C_{phyto} for the NAtl and NPac can be further examined by comparing annual cycles from the satellite record (Figure 2). These data show Chl in the NPac as generally uniform throughout the year, with only a modest ~60% increase from a December minimum of ~0.25 mgChl m^{-3} to a September maximum of ~0.4 mgChl m^{-3} (red symbols, Figure 2a). A much larger range in Chl is observed for the NAtl, with values increasing from a winter minimum of ~0.2 mgChl m^{-3} to a June maximum of 0.7 mgChl m^{-3} (blue symbols, Figure 2a). In contrast, the annual cycles in C_{phyto} for the NPac and NAtl (Figure 2b) exhibit similar winter minima in C_{phyto} of <10 mgC m^{-3} and similar bloom maxima of ~32 mgC m^{-3} for the NPac and ~38 mgC m^{-3} for the NAtl (Figure 2b). Perhaps the most striking difference in the biomass cycles between the NPac and NAtl blooms is their timing. In the NAtl, the springtime rise in C_{phyto} is more rapid and peaks in May/June. The bloom in the NPac is more gradual and has a climax delayed until approximately mid-August.

The interannual variability is much greater than that observed in climatological annual cycles of Chl and C_{phyto}, particularly in the NAtl (supporting information Figure S2). Spatial and temporal binning of satellite products limits the observed variance around each individual 8 day composite. For example, throughout

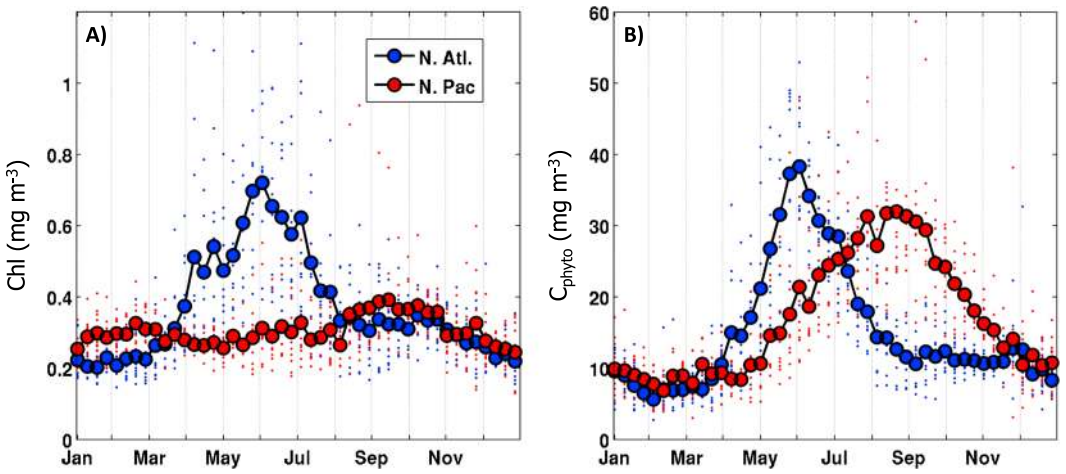

Figure 2. Climatological annual cycles of phytoplankton pigment and carbon biomass in the North Atlantic (large blue circles) and North Pacific (large red circles) Oceans. (a) Chl, mg m^{-3}. (b) C_{phyto}, mg m^{-3}. Climatologies were constructed from weekly (8 day) composites of MODIS data over a 10 year period (2003–1012) averaged over 5° × 10° boxes shown in Figure 1. Small points represent all 8 day data from the 10 year study period.

the 10 year satellite record, values of Chl and C_{phyto} fall within a limited range around climatological average values for the NPac ($CV = \sigma/\overline{Chl} = 0.3 - 0.6$), while in the NAtl large deviations from the average values are frequent ($CV = \sigma/\overline{Chl} = 0.3 - 1.6$). These deviations are particularly large near the bloom climax and give chlorophyll and biomass peaks that often differ from climatological average values by a factor of 4 or more. The limited in situ Chl and C_{phyto} data measured in the field are consistent with this broader range of values (supporting information Figure S2).

Confidence in the annual patterns of satellite retrievals of Chl and C_{phyto} can be gained by examining independent measures of both properties throughout the full annual cycle from in situ autonomous profiling floats. In the NAtl, matchup analyses conducted by *Boss et al.* [2008] have previously shown excellent correspondence between float and satellite-derived Chl and C_{phyto} (see their Figure 3). Since that time, new profiling floats were deployed in the NPac and can be used to "validate" the satellite-inferred patterns. Float-derived C_{phyto} shows the same range of variability as the satellite values and reproduces the annual cycle well in all three years of the deployment (Figures 3a and 3b). Direct matchups between satellite and float C_{phyto} give $r^2 = 0.78$, RMSE = 5.8 mg m^{-3}, an overall mean bias of 2.4 mg m^{-3} (float > satellite), and a mean relative difference of 14% (float > satellite) (Figure 3c). Float-derived Chl shows much more variability than MODISA Chl (supporting information Figure S1). Float-derived Chl also systematically suggests higher values during the late summer period of August–October ($Chl_{float} = 0.53 \pm 0.18$ mg m^{-3}, $Chl_{MODISA} = 0.26 \pm 0.08$ mg m^{-3}). It is possible that this systematic offset is a calibration-related issue and reflects differences between the extant phytoplankton community during this time of year and laboratory chlorophyll standards. No cross-platform calibration of any kind was performed to improve agreement between the float and satellite measurements [e.g., *Boss et al.*, 2008], so the overall correspondence is excellent considering that any comparison of point source field data and satellite pixel level data is inherently difficult.

4. Discussion

Simultaneous observations of satellite Chl and C_{phyto} in the NAtl and NPac suggest a more complicated story than does either record individually. First, satellite Chl is consistent with historical field measurements and supports the view of contrasting seasonal cycles in Chl between the NAtl and NPac. The satellite C_{phyto} product on the other hand suggests the existence of a seasonal phytoplankton bloom in the NPac that is comparable in magnitude to the NAtl, albeit with differences in the timing, spatial heterogeneity, and presumably its underlying controls. This description is inconsistent with traditional views of biomass cycles in the high-latitude Pacific. The following sections attempt to reconcile these observations by examining the role

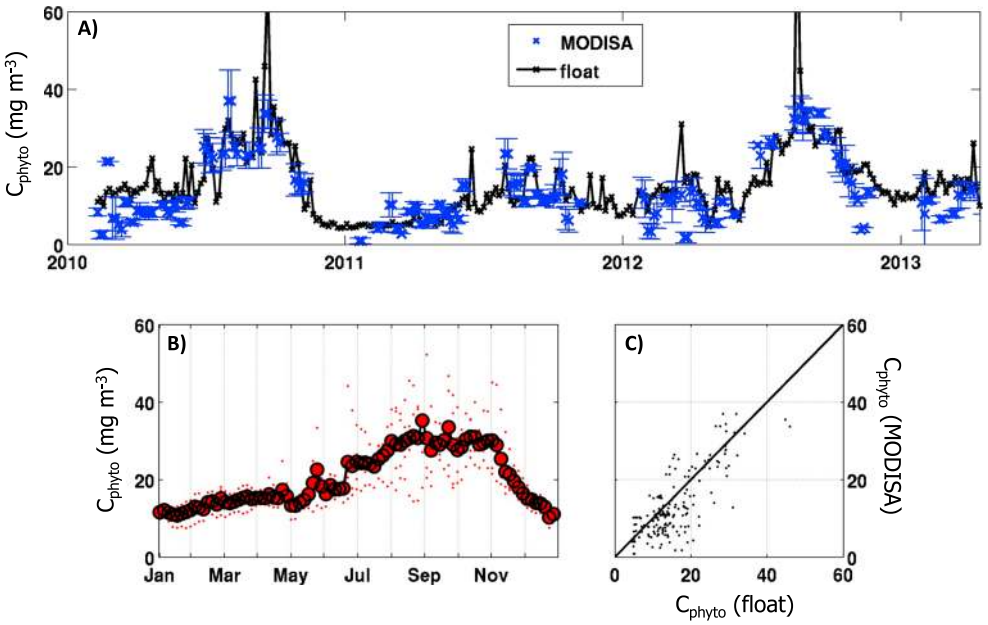

Figure 3. Comparison of float- and satellite-derived estimates of phytoplankton biomass in the NPac. (a) 3^+ year time series of C_{phyto} (mg m^{-3}) spanning 2010 to early 2013 from a single float (black line and symbols). Satellite-derived estimates were taken from nearest MODIS 8 day composite and averaged over a 20 km × 20 km region centered on float location (blue crosses). Variability within this region is shown by the error bars. (b) Multifloat climatological C_{phyto} at 4 day temporal resolution (large red filled circles are climatological average; smaller red dots are individual float and year data). See supporting information Figure S1 for float tracks and lifetimes. (c) Matchup plots between float and satellite C_{phyto}, from a single float shown in panel A ($N = 177$).

of phytoplankton physiology and the balance of growth and loss in shaping patterns in bulk properties such as Chl and C_{phyto}.

4.1. Biomass Versus Physiology: The Carbon to Chlorophyll Ratio

Chlorophyll concentration is a function of both phytoplankton abundance and physiological state (i.e., cellular pigmentation) [*Falkowski and Laroche*, 1991; *Geider et al.*, 1997; *Halsey and Jones*, 2015; *Laws and Bannister*, 1980]. Increases in light exposure or nutrient stress can cause substantial reductions in phytoplankton cellular chlorophyll levels. Conceivably, if these physiological decreases in pigmentation co-occur with net population growth, then it is possible for phytoplankton biomass to increase significantly without concomitant changes in bulk chlorophyll concentration. In other words, the constancy of chlorophyll in the NPac could be accounted for if increases in phytoplankton biomass are offset by physiological changes in cellular pigmentation. To evaluate this potential explanation, it is essential to simultaneously examine both chlorophyll and standing stocks of phytoplankton carbon.

Combining the two satellite products (Chl and C_{phyto}) allows examination of their ratio (denoted hereafter simply as C:Chl, mgC $mgChl^{-1}$), a sensitive metric that registers physiological acclimation to light and nutrient stress (Figure 4). The large-scale latitudinal gradient in climatological spring/summer C:Chl extending from the low latitudes to the subpolar regions reflects such changes in light exposure and nutrient-driven changes in phytoplankton growth rate (and to a lesser degree species composition [*Geider*, 1987]). Focusing on the subpolar regions, widespread values of ~40 mgC $mgChl^{-1}$ are found throughout the NAtl, while values in the NPac are generally between 70 and 120 mgC $mgChl^{-1}$. Low C:Chl (~20 mgC $mgChl^{-1}$) is observed in both subpolar basins during the winter, likely the result of photoacclimation to low incident light levels and deep vertical mixing (Figure 4b, see next section). C:Chl increases slowly through spring and nearly doubles (~35 mgC $mgChl^{-1}$) by the end of April in both the NAtl and NPac (Figure 4b). In the NAtl, C:Chl increases sharply until its maximum in May (~50 mgC $mgChl^{-1}$) and then remains high until mid-July. Values of C:Chl in the NPac continue to increase beyond May until reaching a maximum of nearly 100 at the beginning of August, nearly two months later than the maximum C:Chl observed in the NAtl. Thus, the NPac maximum is nearly twice as large and occurs two months later when compared to the NAtl.

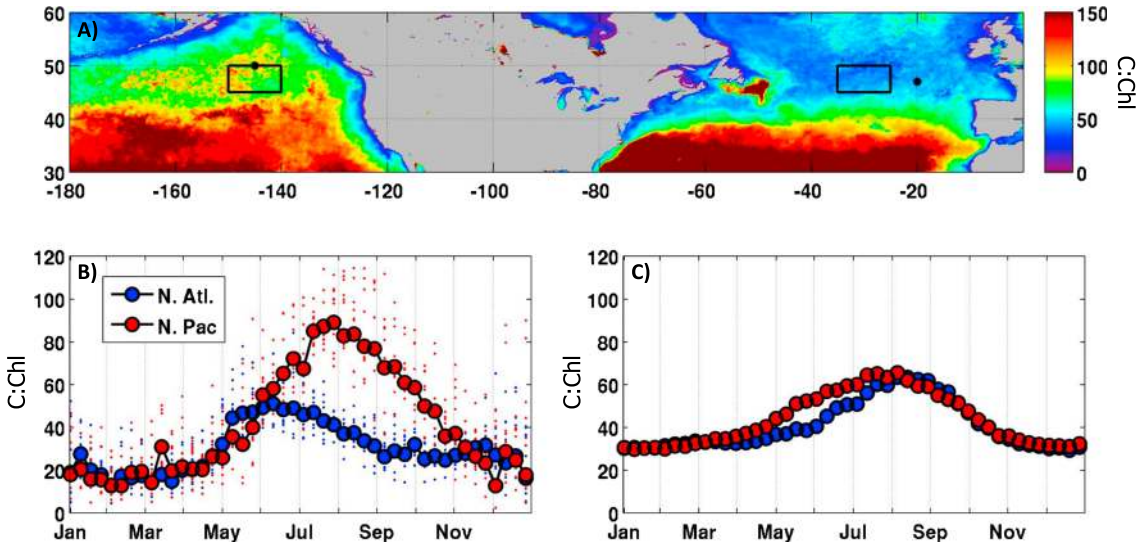

Figure 4. Spatial and temporal patterns in the ratio of phytoplankton biomass to pigment concentration (C:Chl). (a) Climatological spring/summer C:Chl. Values at each pixel are the maximum climatological mean (2003–2012) between April and August from MODIS on Aqua. Black boxes are as shown in Figure 1. (b) Climatological annual cycles of C:Chl in the NAtl (large blue circles) and NPac (large red circles). Small points represent all 8 day data from the 10 year study period. (c) Climatological annual cycles of C:Chl in the NAtl and NPac as predicted from photoacclimation model of *Behrenfeld et al.* [2015].

4.1.1. Light Effects—Photoacclimation

Variability in mixed layer light conditions can be a dominant driver of C:Chl variability. We therefore evaluated the magnitude of this "photoacclimation response" for the NPac and NAtl C:Chl record. The environmental factors that characterize the light regime experienced by phytoplankton and thus the photoacclimation effect on C:Chl are incident light, mixing depth, and light attenuation (Figure 5). Daily cloud-corrected PAR is nearly identical between the two basins, as we would expect at the same latitudes in either ocean, and ranges from ~5 einstein $m^{-2} d^{-1}$ in the winter to ~40 einstein $m^{-2} d^{-1}$ in summer (Figure 5a). There is a small difference during summer months, likely due to persistent cloudiness in the NPac (~10% reduction during July). Mixed layer depths (MLDs) in the NAtl and NPac exhibit very different seasonal patterns, due largely to the existence of a permanent halocline in the NPac. This "freshwater cap" creates strong vertical density gradients which prevent deep convective winter mixing found in the NAtl [*Warren*, 1983]. The seasonal change in NPac MLD is relatively small, and maximal mixing depths rarely exceed 100 m (Figure 5b). In contrast, the difference between winter and summer MLDs in the NAtl is >10×. Summertime MLD is comparable to the NPac (~20 m), but wintertime values can exceed several hundred meters. Lastly, an estimate of the light attenuation (K_{PAR}, m^{-1}) is shown in Figure 5c. Since chlorophyll is often the primary determinant of light attenuation, the annual cycles of K_{PAR} look very similar to Chl. Namely, K_{PAR} is relatively constant ($0.082 \pm 0.003\ m^{-1}$, which corresponds to euphotic depths, Z_{eu}, of 56 ± 2 m) through the year in the NPac. In the NAtl, K_{PAR} increases to $0.12\ m^{-1}$ (Z_{eu}~40 m) through spring and early summer as Chl reaches its maximum then returns to a winter minimum ($0.07\ m^{-1}$ or Z_{eu}~65 m) when Chl is also at its minimum. Together, these quantities define the light availability with depth and can be used to characterize the photophysiology of the phytoplankton community. For example, increases in light availability will decrease cellular pigmentation (higher C:Chl) and may be due to changes in any of the three properties: (1) increases in incident light as the spring/summer progresses, (2) shoaling of the MLD which traps phytoplankton nearer to the sea surface, or (3) decreases in K_{PAR} signaling greater light penetration in the water column. Conversely, a decrease in light exposure will cause an increase in the cellular pigmentation (lower C:Chl) and may be related to decreases in incident light with the approach of Fall/Winter, deepening of the mixed layer exposing the phytoplankton to lower light levels (or even darkness), or an increase in K_{PAR} resulting in greater light attenuation within the water column.

In the NPac, the photoacclimation effect was recognized early on and estimated to change C:Chl by 3–4 times [*Frost*, 1987; *McAllister*, 1969]. This fact alone would be sufficient to conceal a seasonal biomass increase of the same order of magnitude (~3–4 times) in the corresponding Chl record. Therefore, some of the seasonal

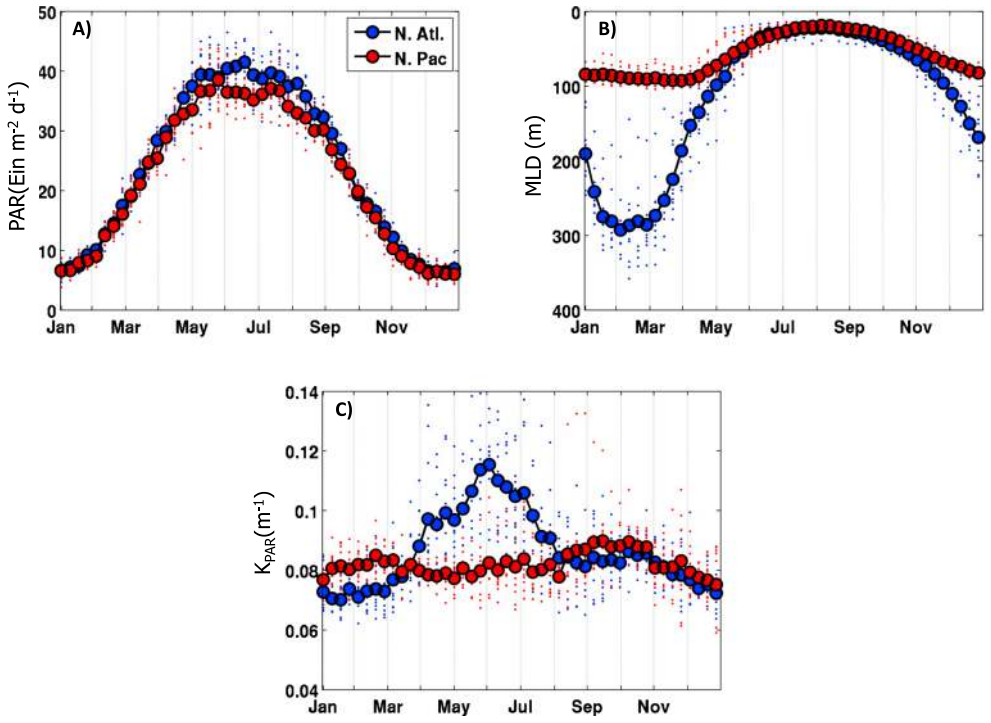

Figure 5. Climatological annual cycles of environmental properties describing the surface ocean light environment in the North Atlantic (large blue circles) and North Pacific (large red circles). (a) Daily integrated broadband irradiance at the sea surface, PAR (einstein m^{-2} d^{-1}). (b) Mixed layer depth, MLD (m). (c) Diffuse attenuation coefficient of PAR, K_{PAR} (m^{-1}). Climatologies were constructed from weekly (8 day) composites of MODIS data over a 10 year period (2003–1012) averaged over 5° × 10° boxes shown in Figure 1. Small points represent all 8 day data from the 10 year study period.

change in C:Chl can be attributed to photoacclimation and we can estimate this effect directly in both basins using the environmental properties of PAR, K_{PAR}, and MLD together with a recent photophysiological model designed to predict C:Chl explicitly [*Behrenfeld et al.*, 2015]. This model has been tested on both field and satellite data and accurately reproduces observed satellite C:Chl in the majority of ocean regions, including

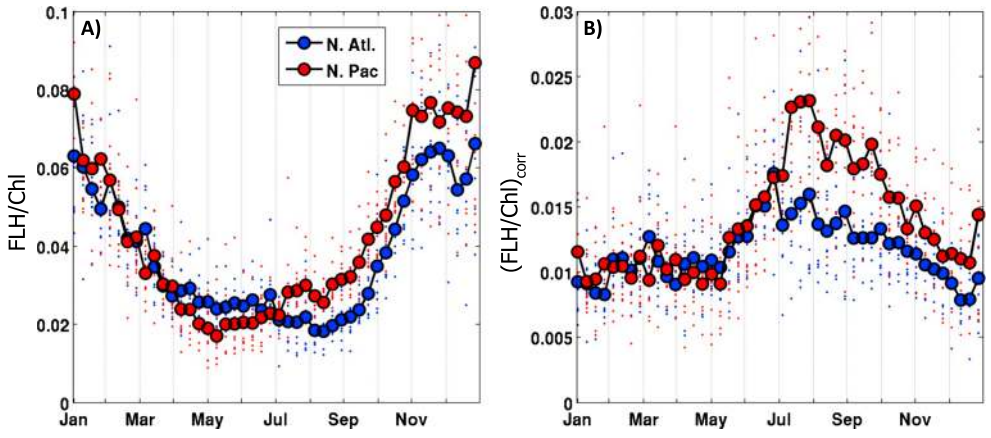

Figure 6. Climatological annual cycles in chlorophyll fluorescence efficiency as an indication of iron stress in the North Atlantic (large blue circles) and North Pacific (large red circles). (a) FLH/Chl fluorescence line height (FLH) normalized to Chl. (b) FLH/Chl corrected for effects of photoacclimation and nonphotochemical quenching. Climatologies were constructed from weekly (8 day) composites of MODIS data over a 10 year period (2003–1012) averaged over 5° × 10° boxes shown in Figure 1. Small points represent all 8 day data from the 10 year study period.

the NAtl. Briefly, the model is consistent at times with past efforts which utilize the median mixed layer light level to define a common acclimation irradiance [e.g., *Behrenfeld et al.*, 2005; *Westberry et al.*, 2008]. However, this relationship is only valid under conditions of shallow mixing (when MLD $< Z_{eu}$). When the MLD exceeds the euphotic depth, (or under any mixing conditions near dawn and dusk) phytoplankton cells will be exposed to complete darkness for some portion of their photoperiod. During this time, the regulatory mechanisms for chlorophyll synthesis actually signal for the cell to stop making chlorophyll (similar to high light), contrary to cellular signals sent/received during low light conditions. Without this consideration, the median mixed layer irradiance by itself will overestimate cellular chlorophyll.

Application of this model to our satellite data set yields seasonal C:Chl that is remarkably similar to one another throughout the year, despite large differences in water column light environments of the two basins (Figure 4c). Two primary factors contribute to this similarity. First, summertime MLD is extremely shallow in both the NAtl and NPac. Combined with high incident irradiances, phytoplankton growing in the summer mixed layer are exposed to supersaturating light levels throughout the day and represent an example of photoacclimation to high light. In the winter, MLD is deep relative to the euphotic depths in both basins and phytoplankton that are photoacclimated to low light. The deeper MLD of the NAtl does not have an additional effect on photoacclimation as it is likely not worth the energetic investment in additional pigment synthesis. The largest divergence between model-predicted patterns of C:Chl in the NAtl and NPac is seen in June when NAtl Chl is maximal, Z_{eu} is minimal, and water transparency is minimal leading to increased cellular pigmentation relative to the NPac (Figure 4c).

Observed and predicted C:Chl in both basins show similarities in the stable, low values through winter and approximate twofold increase through spring and summer. Small differences also exist between observed and predicted C:Chl in the NAtl, but by far the most striking difference is seen in the NPac. The photoacclimation model only captures approximately half of the observed increase in C:Chl during March–August in the NPac.

In other words, photoacclimation causes some, but not all, of the winter through summer increase in C:Chl necessary to account for the observed stability in surface chlorophyll concentrations during this time. Similarly, the twofold increase observed in NAtl C:Chl through the spring dampens the bloom signature in the Chl record.

4.1.2. Nutrient Effects—Iron and Fluorescence

In the subarctic NPac, iron is at limiting levels for many phytoplankton [*Martin and Fitzwater*, 1988; *Martin et al.*, 1990]. Dust is the primary source of new iron in most open ocean locations [*Jickells et al.*, 2005], and lower dissolved iron concentrations in the eastern NPac are consistent with the region's lower dust fluxes relative to the North Atlantic [*Ginoux et al.*, 2001; *Jickells et al.*, 2005]. The NPac exhibits lower Fe:N ratios in upwelling deep water and lower Fe:N in surface phytoplankton [*Fung et al.*, 2000], which is indicative of iron limitation. Iron stress has also been implicated based on biochemical markers (i.e., flavodoxin) in diatoms [*LaRoche et al.*, 1996] and by enhanced nutrient drawdown and biomass accumulation upon addition of iron [*Boyd et al.*, 2005].

Iron availability has broad-reaching effects on phytoplankton physiology, the primary result being growth limitation. Nutrient-driven changes in growth rate—whether caused by iron or otherwise—are accompanied by linearly proportional changes in light-harvesting capacity (i.e., quantified by C:Chl) [*Halsey and Jones*, 2015; *Laws and Bannister*, 1980]. Laboratory studies consistently show that C:Chl is elevated under iron stress [*Greene et al.*, 1992; *Sunda and Huntsman*, 1995]. In a study on four species of *Pseudo-nitzschia* isolated from OSP, cellular C:Chl decreased from 110 mgC mgChl^{-1} under iron limitation to 50 mgC mgChl^{-1} in iron-replete cells [*Marchetti and Harrison*, 2007]. In the field, shipboard incubations of iron-amended natural phytoplankton assemblages from OSP yielded a decrease in C:Chl from ~140 to 25 mgC mgChl^{-1} [*Coale*, 1991]. More striking still are results from the Subarctic Ecosystem Response to Iron Enrichment Study (SERIES), where iron was directly injected into the surface ocean near OSP and C:Chl decreased from 120 to 40 mgC mgChl^{-1} over ~12 days [*Boyd et al.*, 2005, 2004]. Satellite coverage during SERIES was limited due to persistent clouds, but *Westberry et al.* [2013] used available satellite imagery to show that while C_{phyto} increased significantly in the fertilized patch (from 36 ± 9 mg m^{-3} to 117 ± 28 mg m^{-3}), C:Chl decreased by an even greater amount relative to the surrounding waters (see their Figure 9). An example of iron effects on phytoplankton at an even broader scale can be seen in the satellite climatology of C:Chl, where isolated

patches of elevated C:Chl are scattered throughout the eastern NPac (Figure 4a). These features can be traced to a singular iron-related event included in the satellite climatology rather than a recurrent seasonal characteristic of the ecosystem. Specifically, the eruption of Mountain Kasatochi in the Aleutian Islands during August 2008 deposited significant amounts of volcanic ash in the region and has been associated with the highest Chl observed during the satellite era (1997 to present) across the region [*Hamme et al.*, 2010]. Corresponding anomalies in satellite C_{phyto} and the ratio C:Chl are also found during this period (supporting information Figure S3). Taken together, these laboratory, field, and satellite studies demonstrate the prominent role of iron stress on regulation of C:Chl and the importance of physiology in the shaping bulk properties such as Chl.

Iron stress causes unique changes in phytoplankton fluorescence properties that can be routinely monitored in the field and from space [*Behrenfeld et al.*, 2006, 2009; *Ryan-Keogh et al.*, 2013; *Westberry et al.*, 2013]. Iron-stressed, macronutrient-replete phytoplankton exhibit enhanced fluorescence yields (see review by *Behrenfeld and Milligan* [2013]). To detect the iron stress signal, it is first required that the confounding effects of light-dependent nonphotochemical quenching (NPQ) are removed. NPQ results from a broadly expressed set of physiological mechanisms that protect phytoplankton from excess absorbed light and dwarf other forms of environmental and physiological variability in the fluorescence signal. For example, the annual patterns in MODIS chlorophyll fluorescence normalized to pigment biomass (FLH/Chl) in the NAtl and NPac are dominated by the fourfold decrease from winter to summer due to NPQ (Figure 6a). Previous studies using satellite fluorescence have tried to "remove" this signal by employing a fixed correction for NPQ that follows an inverse function of incident light [*Behrenfeld et al.*, 2009; *Westberry et al.*, 2013]. However, NPQ response should also be a function of the phytoplankton photoacclimation "state" [*Behrenfeld et al.*, 2009; *O'Malley et al.*, 2014]. The photophysiological model previously used to estimate C:Chl in section 4.1 can also quantify the photoacclimation state of the phytoplankton community through the light saturation parameter, E_k (supporting information Figure S4; for full details of the model see *Behrenfeld et al.* [2015]). A typical NPQ response curve following an inverse function of light (1/iPAR) can then be weighted by E_k to "correct" the satellite FLH/Chl (Figure 6b). E_k-corrected FLH/Chl shows a steady increase from May to August, consistent with increasing iron stress in the NPac. The twofold winter to summer difference is within the range expected from iron-induced changes to photosystem stoichiometry (i.e., PSII:PSI) [*Ivanov et al.*, 2000; *Ryan-Keogh et al.*, 2013; *Strzepek and Harrison*, 2004]. During the second half of the year, the gradual decline to wintertime values likely reflects the increasing introduction of iron from intermittent mixing events and lateral supply of iron from the continental shelf [*Lam et al.*, 2006]. Interestingly, a similar pattern in E_k-corrected FLH/Chl is seen in the NAtl, although without as significant an increase and with slightly different timing (Figure 6b). This suggestion of seasonal iron limitation in the NAtl is consistent with recent fieldwork demonstrating postbloom iron limitation in the region [*Nielsdottir et al.*, 2009; *Ryan-Keogh et al.*, 2013].

4.1.3. Summary of Physiological Effects on C:Chl

Our results suggest that the role of physiology must be considered when examining Chl records [*Behrenfeld et al.*, 2008; *Siegel et al.*, 2013]. An analogous problem that has been more widely recognized is accounting for photoacclimation and NPQ effects on vertical profiles of chlorophyll fluorescence [*Cullen*, 1982, 2015; *Kitchen and Zaneveld*, 1990]. Outside of this example, however, many applications looking at large-scale patterns or patterns of change in Chl routinely neglect these phenomena [*Boyce et al.*, 2010; *Gregg et al.*, 2005; *Irwin and Oliver*, 2009; *McClain et al.*, 2004; *Polovina et al.*, 2008]. Here we have shown that seasonal photoacclimation can change observed Chl by a factor of 2 or more in the NAtl and NPac without any change in biomass. Furthermore, the combination of light- and nutrient-driven changes in C:Chl may even act in the opposite direction of biomass changes. *Taylor et al.* [1997] demonstrated similar results when examining seasonal and latitudinal variability in C:Chl using a dynamic physiological model [*Geider et al.*, 1997] embedded in a one-dimensional physical model. In addition to light-driven effects, unique consequences of iron stress also impart their signature on C:Chl and further confound interpretations of Chl. These fundamental behaviors are well described in laboratory settings (and to a lesser extent in the field), and we now have the ability to diagnose their effects from satellite ocean color data.

One additional factor which can contribute to broad-scale distributions of C:Chl but not considered here is phytoplankton taxonomic composition. Changes in accessory pigmentation (both photosynthetic and photoprotective) can lead to large differences in the light absorption per unit chlorophyll, a^{CHL} [e.g., *MacIntyre et al.*, 2002]. This finding suggests that a preferred physiological metric to C:Chl would be C:a_{ph},

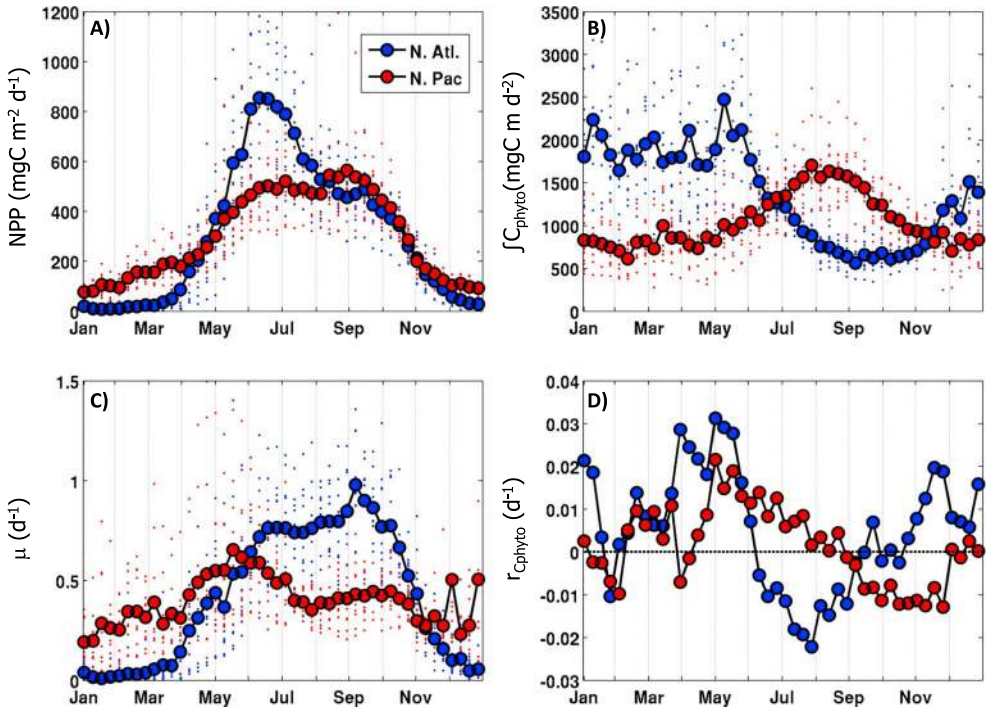

Figure 7. Climatological annual cycles of plankton rates the North Atlantic (blue) and North Pacific (red) Oceans. (a) NPP, mg m^{-2} d^{-1}; (b) water column-integrated biomass ($\int C_{phyto}$), mg m^{-2}; (c) specific growth rate (μ), d^{-1}; and (d) net population growth rate (r) d^{-1}. Climatologies were constructed from weekly (8 day) composites of MODIS data over a 10 year period (2003–1012).

where a_{ph} quantifies phytoplankton absorption [*Babin et al.*, 1996] and could be effected through satellite remote sensing of inherent optical properties.

4.2. Phytoplankton Growth and Accumulation Rate

In order to further develop an understanding of the plankton annual cycle in the NPac, we must consider not only pigment and biomass stocks but also rates of primary production, growth, and biomass accumulation (or net population growth). Here we have used the Carbon-based Production Model (CbPM) [*Westberry et al.*, 2008] to estimate net primary production (NPP, mgC m^{-2} d^{-1}) in the NAtl and NPac (Figure 7a). Similar analyses carried out with the Vertically Generalized Production Model (VGPM) [*Behrenfeld and Falkowski,* 1997] differ somewhat due mostly to the treatment (or lack thereof) of photoacclimation (supporting information Figure S5). In the NAtl, wintertime NPP is extremely low, remaining around 20 ± 10 mgC m^{-2} d^{-1}. Between March and mid-June, NPP rises quickly to a maximum of nearly 850 mgC m^{-2} d^{-1}. From there, NPP initially decreases quickly until August, after which time there is a secondary peak in NPP that extends through mid-September. As in the case with Chl, spatial and temporal averaging dampens interannual variability and the full range of NPP encountered is much larger than reflected in Figure 7a (not shown). Wintertime NPP in the NPac is significantly higher (~100 mgC m^{-2} d^{-1}) and increases slowly and steadily to a sustained maximum that lasts from June to September (~500 mgC m^{-2} d^{-1}). For comparison, in situ measured NPP at OSP ranges from ~100–400 mgC m^{-2} d^{-1} in winter to ~800–1200 mgC m^{-2} d^{-1} in summer and shows considerable interannual variability [see *Boyd and Harrison*, 1999, Figure 7].

In order to estimate algal growth rates (μ, d^{-1}), the total column-integrated phytoplankton biomass ($\int C_{phyto}$) must be known. $\int C_{phyto}$ can be calculated by extrapolating surface C_{phyto} uniformly to the MLD or Z_{eu}, whichever is deeper. The highest biomass in the NAtl is actually found throughout the winter and early spring, owing to extremely deep mixed layer depths (Figure 7b). This observation is supported by the few wintertime shipboard profiles of chlorophyll fluorescence [e.g., *Backhaus et al.*, 2003] and float-derived Chl and C_{phyto} [*Boss and Behrenfeld*, 2010; *Boss et al.*, 2008]. In the second half of the year, column-integrated biomass in the NPac is actually greater than that in the NAtl by as much as twofold or threefold during August and

September. Phytoplankton growth rate (μ, d^{-1}) can be calculated as the ratio of NPP and total biomass (e.g., $\mu = NPP/\int C_{phyto}$). Wintertime μ in the NPac is significantly higher than that in the NAtl because early-season growth rates in the Atlantic are suppressed by the light-limiting effects of deep mixed layers (Figure 7c). Maximum μ in the NPac (~0.65 d^{-1}) never reaches the same magnitude as in the NAtl (~1 d^{-1}). Satellite estimates of μ in the NPac are consistent with the limited field measurements that exist [*Booth et al.*, 1993; *Boyd and Harrison*, 1999; *Landry et al.*, 1993; *Rivkin et al.*, 1999].

The accumulation rate of biomass (r, d^{-1}) is uncoupled from the specific growth rate (μ) due to its inclusion of loss processes. Therefore, we calculate the net biomass accumulation rate r (d^{-1}) as

$$r = \frac{1}{C_{phyto}}\frac{dC_{phyto}}{dt}, \quad \text{if } \frac{dMLD}{dt} < 0 \text{ and } (MLD < Z_{eu})$$
$$= \frac{1}{\int C_{phyto}}\frac{d\int C_{phyto}}{dt}, \quad \text{otherwise}$$

The conditional definition takes into account the effects of dilution on biomass when the mixed layer is deepening [*Behrenfeld and Boss*, 2014]. The annual pattern of biomass accumulation rate in the NAtl has been previously reported by *Behrenfeld* [2010, Figure 4] and shows that r first becomes greater than 0 in the winter, despite extremely low phytoplankton specific growth rates (Figures 7c and 7d). Biomass accumulation ($r > 0$) continues until June, after which time biomass decreases ($r < 0$). The end of biomass accumulation coincides with the highest μ of the year, which persists through summer and into early fall, indicating that loss processes must exceed phytoplankton growth. In the NPac, the annual pattern of r shows some fundamental differences. Most importantly, biomass accumulation continues steadily from winter to the summer months, nearly 2–2.5 months longer than in the NAtl (Figure 7d). This can also be seen in the annual pattern of surface biomass (Figure 2b) and column-integrated biomass (Figure 7a), both of which peak in August and September.

Summarizing these patterns, we find that the NPac is characterized by lower rates of biomass accumulation and a delayed biomass peak compared to the NAtl (Figure 2b). This slow accumulation of biomass reflects a tighter coupling of phytoplankton growth and loss processes (grazing, sinking, lysis, etc.). For example, between February and April, phytoplankton biomass increases only marginally in the NPac and nearly triples in the NAtl, despite higher growth rates in the Pacific (Figure 7a). As previously mentioned, early-season growth rates in the NAtl are kept in check by deep mixing and low light availability, but this same mixing further decouples phytoplankton growth from loss, allowing net biomass accumulation [*Behrenfeld and Boss*, 2014]. Indeed, the comparable (or greater) rates of NPP in the NPac than in NAtl suggest that a smaller fraction of total phytoplankton production accumulates in the Pacific during this period. Quantitatively, less than 1% of phytoplankton production in the NPac is accounted for by biomass accumulation between February and April; the remaining production is consumed by grazers or lost from the mixed layer. In contrast, a greater decoupling of phytoplankton growth and loss in the Atlantic allows ~2.5% of the total production to accumulate as biomass, resulting in an early rise in phytoplankton abundance despite lower growth rates.

4.3. Nitrate Drawdown

In addition to differences in chlorophyll, comparisons of the subarctic oceans often contrast the summertime exhaustion of surface nitrate (NO_3) in the subarctic Atlantic with persistently elevated nitrate levels in the eastern subarctic Pacific. While highlighting an important characteristic of iron-limited environments, such comparisons potentially overlook similarities in nitrate drawdown between the two systems. In the NAtl, NO_3 concentrations are maximal after winter convective mixing (~8 μM in January and February) then are exhausted by midsummer as phytoplankton biomass accumulates and stratification cuts off supply from below (Figure 8a). While the NO_3 pool in the NPac is much larger (wintertime concentrations ~15 μM), the magnitude of spring/summer drawdown (~8 μM) is nearly identical to that observed in the NAtl (Figure 8a). Insufficient iron supply prevents further nitrate drawdown in the subarctic NPac, as demonstrated by additional nutrient depletion and elevated biomass responses to artificially augmented iron supply [*Boyd et al.*, 2005]. Further, the NO_3 depletion rate is nearly twice as fast in the Atlantic as in the Pacific. Several years worth of float-collected NO_3 data in the same area also show a very similar pattern as the climatology and indicate a seasonal drawdown of ~7 μM each year (Figure 8a). Importantly, NO_3 drawdown during the spring/summer in both basins mirrors the associated biomass buildup observed from the satellite record (Figure 8b). These results indicate that the timing of nitrate drawdown in both basins is closely linked to

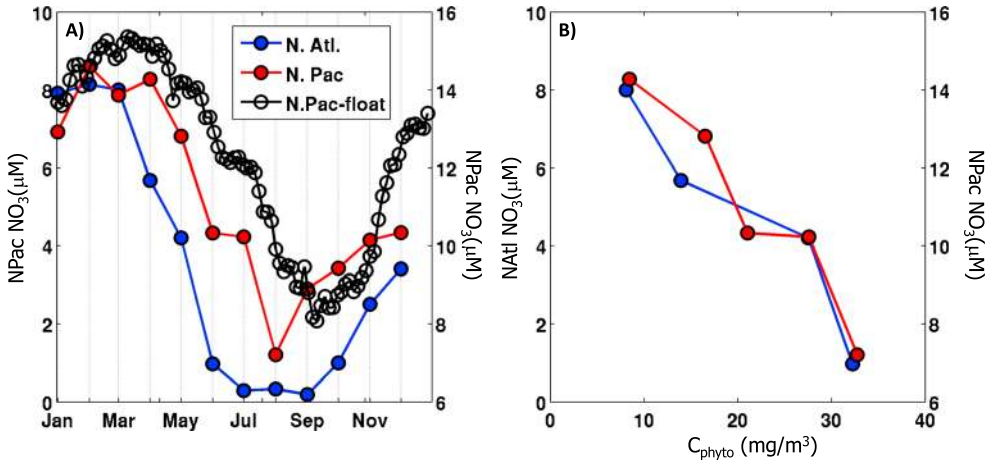

Figure 8. Seasonal nitrate (NO_3) drawdown and biomass accumulation in the North Atlantic (blue) and North Pacific (red) Oceans. (a) Monthly climatological NO_3 taken from the World Ocean Atlas 2009. Also shown is annual cycle of autonomous profiling float-based NO_3 measurements (open circles) in the NPac—data are taken from the MBARI Chemical Sensor Lab, www.mbari.org/chemsensor/FloatList.html, (b) NO_3 versus climatological C_{phyto} during the period of uptake (March–June in Atlantic, April–August in Pacific).

phytoplankton biomass accumulation, yet the observed biomass increase during the spring/summer can only account for <5% of the NO_3 drawdown (assuming a Redfield C:N molar ratio of 106:16). This result further suggests similar levels of new production in the two systems (~600 mgC m^{-3} yr^{-1}). Indeed, total particulate organic carbon flux measurements from deep-moored sediment traps support this conclusion and show that export in the NPac is equal to or even exceeds that in the NAtl [*Wong et al.*, 1999].

4.4. Summary

Variability in C:Chl has been largely neglected in previous comparisons of phytoplankton dynamics in the North Atlantic and Northeast Pacific. Consequently, regional differences in chlorophyll have led to the long-standing question, "What factors prevent phytoplankton from accumulating in the North Pacific?" However, satellite-based phytoplankton carbon retrievals contradict the notion of diminished phytoplankton biomass in the North Pacific. Based on these findings, we suggest that the quintessential spring chlorophyll bloom in the North Atlantic is a consequence of coincident maxima in both phytoplankton carbon biomass and cellular chlorophyll (i.e., low C:Chl). The seasonal cycle in the North Pacific, on the other hand, is in direct opposition to this pattern, with increases in biomass accompanied by decreases in cellular chlorophyll. Consequently, summertime chlorophyll concentrations are low despite biomass levels that are comparable to the North Atlantic spring bloom. This revelation emphasizes the importance of physiological variability on bloom attributes and highlights one of the dangers in characterizing ocean ecosystems based on chlorophyll properties alone.

While our results contradict the notion of persistently low phytoplankton biomass in the eastern subarctic Pacific, they do not contradict notions of the subarctic Pacific ecosystem's constraint on net population growth. Indeed, the consensus view of iron stress and tight phytoplankton-grazer coupling is surely integral to the slow, 8 month rise in biomass. Only a slightly weaker link between phytoplankton growth and grazing losses is needed to accommodate the observed changes in biomass, relative to traditional views. This minor adjustment nevertheless causes the difference between seasonal phytoplankton accumulations in the subarctic Pacific contrasting with or being comparable to those of other global ocean provinces.

Acknowledgments
This work was supported by NASA grants NNX08AK70G and NNX11AE64G. The authors would like to thank Ken Johnson and Emmanuel Boss for sharing float data publicly. Many of the ideas in this work were developed as part of P.S. PhD dissertation.

References

Babin, M., A. Morel, and B. Gentili (1996), Remote sensing of sea surface sun-induced chlorophyll fluorescence: Consequences of natural variations in the optical characteristics of phytoplankton and the quantum yield of chlorophyll a fluorescence, *Int. J. Remote Sens.*, *17*(12), 2417–2448.

Backhaus, J. O., E. N. Hegseth, H. Wehde, X. Irigoien, K. Hatten, and K. Logemann (2003), Convection and primary production in the winter, *Mar. Ecol. Prog. Ser.*, *251*, 1–14.

Behrenfeld, M. J. (2010), Abandoning Sverdrup's critical depth hypothesis on phytoplankton blooms, *Ecology*, *91*(4), 977–989.

Behrenfeld, M. J., and E. S. Boss (2014), Resurrecting the ecological underpinnings of ocean plankton blooms, *Annu. Rev. Mar. Sci.*, *6*, 167–194.
Behrenfeld, M. J., and P. G. Falkowski (1997), Photosynthetic rates derived from satellite-based chlorophyll concentration, *Limnol. Oceanogr.*, *42*(1), 1–20.
Behrenfeld, M. J., and A. J. Milligan (2013), Photophysiological expressions of iron stress in phytoplankton, in *Annual Review of Marine Science*, vol. 5, edited by C. A. Carlson and S. J. Giovannoni, pp. 217–246, Annual Reviews, Palo Alto, Calif.
Behrenfeld, M. J., E. Boss, D. A. Siegel, and D. M. Shea (2005), Carbon-based ocean productivity and phytoplankton physiology from space, *Global Biogeochem. Cycles*, *19*, GB1006, doi:10.1029/2004GB002299.
Behrenfeld, M. J., K. Worthington, R. M. Sherrell, F. P. Chavez, P. Strutton, M. McPhaden, and D. M. Shea (2006), Controls on tropical Pacific Ocean productivity revealed through nutrient stress diagnostics, *Nature*, *442*(7106), 1025–1028.
Behrenfeld, M. J., K. H. Halsey, and A. J. Milligan (2008), Evolved physiological responses of phytoplankton to their integrated growth environment, *Philos. Trans. R. Soc. London, Ser. B*, *363*(1504), 2687–2703.
Behrenfeld, M. J., et al. (2009), Satellite-detected fluorescence reveals global physiology of ocean phytoplankton, *Biogeosciences*, *6*, 779–794.
Behrenfeld, M. J., S. C. Doney, I. Lima, E. S. Boss, and D. A. Siegel (2013), Annual cycles of ecological disturbance and recovery underlying the subarctic Atlantic spring plankton bloom, *Global Biogeochem. Cycles*, *27*, 526–540, doi:10.1002/gbc.20050.
Behrenfeld, M. J., R. T. O'Malley, E. Boss, T. K. Westberry, J. R. Graff, K. H. Halsey, A. J. Milligan, D. A. Siegel, and M. B. Brown (2015), Revaluating ocean warming impacts on global phytoplankton, *Nat. Clim. Change*, doi:10.1038/nclimate2838.
Bleck, R. (2002), An oceanic general circulation model framed in hybrid isopycnic-Cartesian coordinates, *Ocean Model.*, *4*(1), 55–88.
Booth, B. C., J. Lewin, and J. R. Postel (1993), Temporal variation in the structure of autotrophic and heterotrophic communities in the sub-arctic Pacific, *Prog. Oceanogr.*, *32*(1–4), 57–99.
Boss, E., and M. Behrenfeld (2010), In situ evaluation of the initiation of the North Atlantic phytoplankton bloom, *Geophys. Res. Lett.*, *37*, L18603, doi:10.1029/2010GL044174.
Boss, E., and W. S. Pegau (2001), Relationship of light scattering at an angle in the backward direction to the backscattering coefficient, *Appl. Optics*, *40*(30), 5503–5507.
Boss, E., D. Swift, L. Taylor, P. Brickley, R. Zaneveld, S. Riser, M. J. Perry, and P. G. Strutton (2008), Observations of pigment and particle distributions in the western North Atlantic from an autonomous float and ocean color satellite, *Limnol. Oceanogr.*, *53*(5), 2112–2122.
Boyce, D. G., M. R. Lewis, and B. Worm (2010), Global phytoplankton decline over the past century, *Nature*, *466*(7306), 591–596.
Boyd, P., and P. J. Harrison (1999), Phytoplankton dynamics in the NE subarctic Pacific, *Deep Sea Res., Part II*, *46*(11–12), 2405–2432.
Boyd, P. W., P. J. Harrison, and B. D. Johnson (1999), The joint global ocean flux study (Canada) in the NE subarctic Pacific, *Deep Sea Res., Part II*, *46*(11–12), 2345–2350.
Boyd, P. W., et al. (2004), The decline and fate of an iron-induced subarctic phytoplankton bloom, *Nature*, *428*(6982), 549–553.
Boyd, P. W., et al. (2005), The evolution and termination of an iron-induced mesoscale bloom in the northeast subarctic Pacific, *Limnol. Oceanogr.*, *50*(6), 1872–1886.
Brody, S. R., and M. S. Lozier (2014), Changes in dominant mixing length scales as a driver of subpolar phytoplankton bloom initiation in the North Atlantic, *Geophys. Res. Lett.*, *41*, 3197–3203, doi:10.1002/2014GL059707.
Broecker, W. S. (1991), The great ocean conveyor, *Oceanography*, *4*(2), 79–89.
Broecker, W. S., and G. H. Denton (1990), The role of ocean–atmosphere reorganizations in glacial cycles, *Quat. Sci. Rev.*, *9*(4), 305–341.
Carton, J. A., G. Chepurin, and X. H. Cao (2000a), A simple ocean data assimilation analysis of the global upper ocean 1950–95. Part II: Results, *J. Phys. Oceanogr.*, *30*(2), 311–326.
Carton, J. A., G. Chepurin, X. H. Cao, and B. Giese (2000b), A simple ocean data assimilation analysis of the global upper ocean 1950–95. Part I: Methodology, *J. Phys. Oceanogr.*, *30*(2), 294–309.
Chiswell, S. M., P. H. R. Calil, and P. W. Boyd (2015), Spring blooms and annual cycles of phytoplankton: A unified perspective, *J. Plankton Res.*, *37*(3), 500–508.
Clancy, R. M., and W. D. Sadler (1992), The fleet numerical oceanography center suite of oceanographic models and products, *Weather Forecasting*, *7*(2), 307–327.
Coale, K. H. (1991), Effects of iron, manganese, copper, and zinc enrichments on productivity and biomass in the sub-arctic Pacific, *Limnol. Oceanogr.*, *36*(8), 1851–1864.
Colebrook, J. M. (1982), Continuous plankton records—Seasonal variations in the distribution and abundance of plankton in the North Atlantic Ocean and the North Sea, *J. Plankton Res.*, *4*(3), 435–462.
Cullen, J. J. (1982), The deep chlorophyll maximum—Comparing vertical profiles of chlorophyll *a*, *Can. J. Fish. Aquat. Sci.*, *39*(5), 791–803.
Cullen, J. J. (2015), Subsurface chlorophyll maximum layers: Enduring enigma or mystery solved?, *Annu. Rev. Mar. Sci.*, *7*, 207–239.
Dall'Olmo, G., T. K. Westberry, M. J. Behrenfeld, E. Boss, and W. H. Slade (2009), Significant contribution of large particles to optical backscattering in the open ocean, *Biogeosciences*, *6*(6), 947--967.
Evans, G. T., and J. S. Parslow (1985), A model of annual plankton cycles, *Biol. Oceanogr.*, *3*(3), 327–347.
Falkowski, P. G., and J. Laroche (1991), Acclimation to spectral irradiance in algae, *J. Phycol.*, *27*(1), 8–14.
Freeland, H. (2007), A short history of ocean station papa and line P, *Prog. Oceanogr.*, *75*(2), 120–125.
Frost, B. W. (1987), Grazing control of phytoplankton stock in the open sub-arctic Pacific Ocean—A model assessing the role of mesozooplankton, particularly the large calanoid copepods *Neocalanus* spp, *Mar. Ecol. Prog. Ser.*, *39*(1), 49–68.
Fung, I. Y., S. K. Meyn, I. Tegen, S. C. Doney, J. G. John, and J. K. B. Bishop (2000), Iron supply and demand in the upper ocean, *Global Biogeochem. Cycles*, *14*(1), 281–295, doi:10.1029/1999GB900059.
Garcia, H. E., R. A. Locarnini, T. P. Boyer, J. I. Antonov, M. M. Zweng, O. K. Baranova, and D. R. Johnson (2010), *World Ocean Atlas 2009, Volume 4: Nutrients (Phosphate, Nitrate, Silicate)*, edited by S. Levitus, 398 pp., U.S. Gov. Print. Off., Washington, D. C.
Geider, R. J. (1987), Light and temperature dependence of the carbon to chlorophyll a ratio in microalgae and cyanobacteria: Implications for physiology and growth of phytoplankton, *New Phytol.*, *106*(1), 1–34.
Geider, R. J., H. L. MacIntyre, and T. M. Kana (1997), Dynamic model of phytoplankton growth and acclimation: Responses of the balanced growth rate and the chlorophyll a: Carbon ratio to light, nutrient-limitation and temperature, *Mar. Ecol. Progr. Ser.*, *148*(1–3), 187–200.
Ginoux, P., M. Chin, I. Tegen, J. M. Prospero, B. Holben, O. Dubovik, and S. J. Lin (2001), Sources and distributions of dust aerosols simulated with the GOCART model, *J. Geophys. Res.*, *106*(D17), 20,255–20,273, doi:10.1029/2000JD000053.
Graff, J. R., A. J. Milligan, and M. J. Behrenfeld (2012), The measurement of phytoplankton biomass using flow-cytometric sorting and elemental analysis of carbon, *Limnol. Oceanogr. Meth.*, *10*, 910–920.
Graff, J. R., T. K. Westberry, A. J. Milligan, M. B. Brown, G. Dall'Olmo, V. van Dongen-Vogels, K. M. Reifel, and M. J. Behrenfeld (2015), Analytical phytoplankton carbon measurements spanning diverse ecosystems, *Deep Sea Res., Part I*, *102*, 16–25.

Gran, H. H., and T. Braarud (1935), A quantitative study on the phytoplankton of the Bay of FUndy and the Gulf of Maine (including observations on hydrography, chemistry, and morbidity), *J. Biol. Board Canada*, *1*, 219–467.
Greene, R. M., R. J. Geider, Z. Kolber, and P. G. Falkowski (1992), Iron-induced changes in light harvesting and photochemical energy-conversion processes in eukaryotic marine-algae, *Plant Physiol.*, *100*(2), 565--575.
Gregg, W. W., N. W. Casey, and C. R. McClain (2005), Recent trends in global ocean chlorophyll, *Geophys. Res. Lett.*, *32*, L03606, doi:10.1029/2004GL021808.
Halsey, K. H., and B. M. Jones (2015), Phytoplankton strategies for photosynthetic energy allocation, *Annu. Rev. Mar. Sci.*, *7*, 265–297.
Hamme, R. C., et al. (2010), Volcanic ash fuels anomalous plankton bloom in subarctic northeast Pacific, *Geophys. Res. Lett.*, *37*, L19604, doi:10.1029/2010GL044629.
Harrison, P. J. (2002), Station papa time series: Insights into ecosystem dynamics, *J. Oceanogr.*, *58*(2), 259–264.
Henson, S. A., J. P. Dunne, and J. L. Sarmiento (2009), Decadal variability in North Atlantic phytoplankton blooms, *J. Geophys. Res.*, *114*, C04013, doi:10.1029/2008JC005139.
Irwin, A. J., and M. J. Oliver (2009), Are ocean deserts getting larger? *Geophys. Res. Lett.*, *36*, L18609, doi:10.1029/2009GL039883.
Ivanov, A. G., Y. I. Park, E. Miskiewicz, J. A. Raven, N. P. A. Huner, and G. Oquist (2000), Iron stress restricts photosynthetic intersystem electron transport in Synechococcus sp, PCC 7942, *Febs Lett.*, *485*(2–3), 173–177.
Jickells, T. D., et al. (2005), Global iron connections between desert dust, ocean biogeochemistry, and climate, *Science*, *308*(5718), 67–71.
Johnson, K. S., S. C. Riser, and D. M. Karl (2010), Nitrate supply from deep to near-surface waters of the North Pacific subtropical gyre, *Nature*, *465*(7301), 1062–1065.
Kitchen, J. C., and J. R. V. Zaneveld (1990), On the noncorrelation of the vertical structure of light-scattering and chlorophyll-a in case I waters, *J. Geophys. Res.*, *95*(C11), 20,237–20,246, doi:10.1029/JC095iC11p20237.
Koeller, P., et al. (2009), Basin-scale coherence in phenology of shrimps and phytoplankton in the North Atlantic Ocean, *Science*, *324*(5928), 791–793.
Lam, P. J., J. K. B. Bishop, C. C. Henning, M. A. Marcus, G. A. Waychunas, and I. Y. Fung (2006), Wintertime phytoplankton bloom in the subarctic Pacific supported by continental margin iron, *Global Biogeochem. Cycles*, *20*, GB1006, doi:10.1029/2005GB002557.
Landry, M. R., B. C. Monger, and K. E. Selph (1993), Time-dependency of microzooplankton grazing and phytoplankton growth in the sub-arctic Pacific, *Prog. Oceanogr.*, *32*(1–4), 205–222.
LaRoche, J., P. W. Boyd, R. M. L. McKay, and R. J. Geider (1996), Flavodoxin as an in situ marker for iron stress in phytoplankton, *Nature*, *382*(6594), 802–805.
Laws, E. A., and T. T. Bannister (1980), Nutrient-limited and light-limited growth of Thalassiosira-fluviatilis in continuous culture, with implications for phytoplankton growth in the ocean, *Limnol. Oceanogr.*, *25*(3), 457–473.
MacIntyre, H. L., T. M. Kana, T. Anning, and R. J. Geider (2002), Photoacclimation of photosynthesis irradiance response curves and photosynthetic pigments in microalgae and cyanobacteria, *J. Phycol.*, *38*(1), 17–38.
Marchetti, A., and P. J. Harrison (2007), Coupled changes in the cell morphology and the elemental (C, N, and Si) composition of the pennate diatom Pseudo-nitzschia due to iron deficiency, *Limnol. Oceanogr.*, *52*(5), 2270–2284.
Maritorena, S., D. A. Siegel, and A. R. Peterson (2002), Optimization of a semianalytical ocean color model for global-scale applications, *Appl. Optics*, *41*(15), 2705–2714.
Martin, J. H., and S. E. Fitzwater (1988), Iron-deficiency limits phytoplankton growth in the Northeast Pacific Subarctic, *Nature*, *331*(6154), 341–343.
Martin, J. H., W. W. Broenkow, S. E. Fitzwater, and R. M. Gordon (1990), Does iron really limit phytoplankton production in the offshore sub-arctic Pacific—Yes, it does: A reply, *Limnol. Oceanogr.*, *35*(3), 775–777.
Martinez, E., D. Antoine, F. D'Ortenzio, and C. d. B. Montegut (2011), Phytoplankton spring and fall blooms in the North Atlantic in the 1980s and 2000s, *J. Geophys. Res.*, *116*, C11029, doi:10.1029/2010JC006836.
McAllister, C. D. (1969), Aspects of estimating zooplankton production from phytoplankton production, *J. Fish. Res. Board Can.*, *26*(2), 199−220.
McClain, C. R., S. R. Signorini, and J. R. Christian (2004), Subtropical gyre variability observed by ocean-color satellites, *Deep Sea Res., Part II*, *51*(1–3), 281–301.
Miller, C. B., B. W. Frost, P. A. Wheeler, M. R. Landry, N. Welschmeyer, and T. M. Powell (1991), Ecological dynamics in the sub-arctic Pacific, a possibly iron-limited ecosystem, *Limnol. Oceanogr.*, *36*(8), 1600–1615.
Morel, A., Y. Huot, B. Gentili, P. J. Werdell, S. B. Hooker, and B. A. Franz (2007), Examining the consistency of products derived from various ocean color sensors in open ocean (case 1) waters in the perspective of a multi-sensor approach, *Remote Sens. Environ.*, *111*(1), 69–88.
Nielsdottir, M. C., C. M. Moore, R. Sanders, D. J. Hinz, and E. P. Achterberg (2009), Iron limitation of the postbloom phytoplankton communities in the Iceland Basin, *Global Biogeochem. Cycles*, *23*, GB3001, doi:10.1029/2008GB003410.
O'Malley, R. T., M. J. Behrenfeld, T. K. Westberry, A. J. Milligan, S. Shang, and J. Yan (2014), Geostationary satellite observations of dynamic phytoplankton photophysiology, *Geophys. Res. Lett.*, *41*, 5052–5059, doi:10.1002/2014GL060246.
Parsons, T. R., and C. M. Lalli (1988), Comparative oceanic ecology of the plankton communities of the subarctic Atlantic and Pacific Oceans, *Oceanogr. Mar. Biol.*, *26*, 317–359.
Platt, T., C. Fuentes-Yaco, and K. T. Frank (2003), Spring algal bloom and larval fish survival, *Nature*, *423*(6938), 398–399.
Polovina, J. J., E. A. Howell, and M. Abecassis (2008), Ocean's least productive waters are expanding, *Geophys. Res. Lett.*, *35*, L03618, doi:10.1029/2007GL031745.
Rivkin, R. B., J. N. Putland, M. R. Anderson, and D. Deibel (1999), Microzooplankton bacterivory and herbivory in the NE subarctic Pacific, *Deep Sea Res., Part II*, *46*(11–12), 2579–2618.
Ryan-Keogh, T. J., A. I. Macey, M. C. Nielsdottir, M. I. Lucas, S. S. Steigenberger, M. C. Stinchcombe, E. P. Achterberg, T. S. Bibby, and C. M. Moore (2013), Spatial and temporal development of phytoplankton iron stress in relation to bloom dynamics in the high-latitude North Atlantic Ocean, *Limnol. Oceanogr.*, *58*(2), 533–545.
Siegel, D. A., S. Maritorena, N. B. Nelson, M. J. Behrenfeld, and C. R. McClain (2005), Colored dissolved organic matter and its influence on the satellite-based characterization of the ocean biosphere, *Geophys. Res. Lett.*, *32*, L20605, doi:10.1029/2005GL024310.
Siegel, D. A., et al. (2013), Regional to global assessments of phytoplankton dynamics from the SeaWiFS mission, *Remote Sens. Environ.*, *135*, 77–91.
Strzepek, R. F., and P. J. Harrison (2004), Photosynthetic architecture differs in coastal and oceanic diatoms, *Nature*, *431*(7009), 689–692.
Sunda, W. G., and S. A. Huntsman (1995), Iron uptake and growth limitation in oceanic and coastal phytoplankton, *Mar. Chem.*, *50*(1–4), 189–206.
Sverdrup, H. (1953), On conditions for the vernal blooming of phytoplankton, *J. Cons. Int. Explor. Mer.*, *18*, 287–295.

Takahashi, T., T. T. Takahashi, and S. C. Sutherland (1995), An assessment of the role of the North Atlantic as a CO2 sink, *Philos. Trans. R. Soc. London, Ser. B*, *348*(1324), 143–151.

Takahashi, T., et al. (2009), Climatological mean and decadal change in surface ocean pCO(2), and net sea-air CO2 flux over the global oceans, *Deep Sea Res., Part II*, *56*(8–10), 554–577.

Taylor, A. H., R. J. Geider, and F. J. H. Gilbert (1997), Seasonal and latitudinal dependencies of phytoplankton carbon-to-chlorophyll a ratios: Results of a modelling study, *Mar. Ecol. Progr. Ser.*, *152*(1–3), 51--66.

Taylor, J. R., and R. Ferrari (2011), Shutdown of turbulent convection as a new criterion for the onset of spring phytoplankton blooms, *Limnol. Oceanogr.*, *56*(6), 2293–2307.

Warren, B. A. (1983), Why is no deep water formed in the North Pacific, *J. Mar. Res.*, *41*(2), 327–347.

Westberry, T., M. J. Behrenfeld, D. A. Siegel, and E. Boss (2008), Carbon-based primary productivity modeling with vertically resolved photoacclimation, *Global Biogeochem. Cycles*, *22*, GB2024, doi:10.1029/2007GB003078.

Westberry, T. K., M. J. Behrenfeld, A. J. Milligan, and S. C. Doney (2013), Retrospective satellite ocean color analysis of purposeful and natural ocean iron fertilization, *Deep Sea Res., Part II*, *73*, 1–16.

Whitney, F. A., and H. J. Freeland (1999), Variability in upper-ocean water properties in the NE Pacific Ocean, *Deep Sea Res., Part II*, *46*(11–12), 2351–2370.

Wong, C. S., F. A. Whitney, D. W. Crawford, K. Iseki, R. J. Matear, W. K. Johnson, and J. S. Page (1999), Seasonal and interannual variability in particle fluxes of carbon, nitrogen and silicon from time series of sediment traps at Ocean Station P, 1982–1993: Relationship to changes in subarctic primary productivity, *Deep Sea Res., Part II*, *46*(11–12), 2735–2760.

Erratum

In the originally published version of this article, two names in the author list were transposed. Michael J. Behrenfeld was listed as the second author, and Patrick Schultz was listed as the third author. This error has since been corrected, and this version may be considered the authoritative version of record.